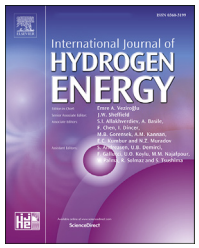
Available online at www.sciencedirect.com

ScienceDirect

journal homepage: www.elsevier.com/locate/he



Cobalt nanoparticles supported on alumina nanofibers (Co/Al_2O_3): Cost effective catalytic system for the hydrolysis of methylamine borane

Ismail Burak Baguc [a], *Mehmet Yurderi* [a], *Ahmet Bulut* [a], *Metin Celebi* [a], *Gulsah Saydan Kanberoglu* [a], *Mehmet Zahmakiran* [a,*], *Murat Kaya* [b], *Murat Aydemir* [c], *Feyyaz Durap* [c], *Akın Baysal* [c]

[a] *Nanomaterials and Catalysis Research Group, Department of Chemistry, Van Yuzuncu Yil University, 65080, Campus, Van, Turkey*

[b] *Department of Chemical Engineering and Applied Chemistry, Atilim University, 06836, Ankara, Turkey*

[c] *Department of Chemistry, Dicle University, 21280, Diyarbakır, Turkey*

ARTICLE INFO

Article history:
Received 7 January 2019
Received in revised form
10 February 2019
Accepted 12 February 2019
Available online 6 March 2019

Keywords:
Methylamine-borane
Hydrogen
Cobalt
Nanoparticles
Alumina nanofiber

ABSTRACT

Amongst different amine-borane derivatives, methylamine-borane ($CH_3NH_2BH_3$) seems to be one of the capable aspirants in the storing of hydrogen attributable to its high hydrogen capacity, stability and aptitude to generate hydrogen through its catalytic hydrolysis reaction under ambient conditions. In this research paper, we report that cobalt nanoparticles supported on alumina nanofibers (Co/Al_2O_3) are acting as active nanocatalyst for catalytic hydrolysis of methylamine-borane. Co/Al_2O_3 nanocatalyst was fabricated by double-solvent method followed with wet-chemical reduction, and was characterized by utilizing various spectroscopic methods and imaging techniques. The results gathered from these analyses showed that the formation Al_2O_3 nanofibers supported cobalt(0) nanoparticles with a mean diameter of 3.9 ± 1.2 nm. The catalytic feat of these cobalt nanoparticles was scrutinized in the catalytic hydrolysis of methylamine-borane by considering their activity and durability performances. They achieve releasing of 3.0 equivalent of H_2 via methylamine-borane hydrolysis at room temperature (*initial* TOF = 297 mol H_2/mol metal × h). Along with activity the catalytic durability of Co/Al_2O_3 was also studied by carrying out recyclability tests and it was found that these supported cobalt nanoparticles have good durability during the course of the catalytic recycles so that Co/Al_2O_3 preserves almost its innate activity at 5th catalytic recycle. The studies presented here also contains kinetic investigation of Co/Al_2O_3 catalyzed methylamine borane hydrolysis depending on the temperature, cobalt and methylamine borane concentrations, which were used to define rate expression and the activation energy of the catalytic reaction.

© 2019 Hydrogen Energy Publications LLC. Published by Elsevier Ltd. All rights reserved.

* *Corresponding author.*
E-mail address: zmehmet@yyu.edu.tr (M. Zahmakiran).
URL: http://www.nanomatcat.com

https://doi.org/10.1016/j.ijhydene.2019.02.088
0360-3199/© 2019 Hydrogen Energy Publications LLC. Published by Elsevier Ltd. All rights reserved.

Introduction

Today, the advancement of secure and effectual hydrogen (H_2) storage is crucial concern in the hydrogen based energy economy, which would aid the changeover from fossil fuel based energy to renewable energy [1,2]. In this respect, the accelerated number of studies are still reported for testing various materials such as carbon nanotubes [3], zeolites [4], metal-organic framework materials [5], organic polymers [6,]hydrous hydrazine ($N_2H_4.H_2O$) [7], boron hydrides ($LiBH_4$, $NaBH_4$, *etc.*) [8], boron-nitrogen compounds (AB; NH_3BH_3, $N_2H_4BH_3$, $NH_3B_3H_7$, *etc.*) [9–12] in the chemical hydrogen storage [13]. Amid these chemicals ammonia-borane (NH_3BH_3) appears to be well-matched for this goal owing to its hydrogen content (19.6 % wt) and benign nature [14]. There are vast numbers of studies have already presented for the ammonia-borane dehydrogenation [9,14,15]; however, an only limited number of reports exist for the dehydrogenation of aqueous methyl substituted AB, methylamine-borane (MeAB; $CH_3NH_2BH_3$) [16–26], which also has high hydrogen content (11.1 % wt). Hydrogen can be generated from MeAB through its catalytic dehydrocoupling in organic solvents [16], hydrolysis in water [17–25] and thermolysis [27] in the absence of solvents. In the midst of these transformations, the metal-catalyzed hydrolysis of MeAB (Eq. (1)) has been known as the most efficient way to produce high purity of H_2 at desirable rates. The studies carried out for the catalytic hydrolysis of MeAB have exposed that 3 mol of H_2 can be released from 1 mol of MeAB (Eq. (1)) under air at room temperature by employing a proper catalytic system.

$$CH_3NH_2BH_3 + 2H_2O \rightarrow CH_3NH_3BO_2 + 3H_2 \quad (1)$$

The literature survey shows that different transition metals based solid supported (Ag@CoNi/graphene [17], Cu@Co/r-GO [18], Ag@Co/graphene [19], Ag@Ni/graphene [19], Ag@Fe/graphene [19], Ru@Ni/graphene [20], Ru@Co/graphene [21], Ru/MCM-41 [22], Ru/CNF [23], Cu/nano-MIL-101 [24], Rh/ZrO_2 [25]) and colloidal (PVP stabilized Ru [26]) nanoparticle (NP) have been employed in MeAB hydrolysis. As seen from the earlier efforts, employed catalytic systems comprises transition metal nanoparticles, which have high surface-to-volume ratio with respect to their bulk counterparts, thus, higher fraction of catalytically active atoms exist on their surface [28]. These highly active catalytic architectures are considered as thermodynamically unstable against to agglomeration into bulk form owing to their large surface areas and high surface energies. In this context, the suitable protecting ligands or polymers are commonly used as stabilizing agents in their synthesis to circumvent their aggregation [29]. Though, the agglomeration of transition metal nanoparticles ultimately to the bulk form even in the attendance of best stabilizing agents [30] is still the most vital concern that should be overwhelmed in their catalytic applications. Additionally, it is one more critical matter to attain neat active metal surfaces by staying away from surface contamination resulting from surface protecting groups, which often lead to a decrease in the catalytic activity resulting from the blocking of active sites. At this concern, the utilization of solid support materials as host material for the immobilization of guest transition metal nanoparticles allows the generation of specific surfactant-free active sites with the advantages of preventing particle aggregation [28–30]. Among these aforementioned nanocatalyst systems employed in the catalytic hydrolysis of MeAB remarkable catalytic activities were achieved by Ru and Rh based NPs; however, the anxieties over the extensive use of these highly expensive metals have driven the studies for the progress of nanocatalysts comprised of low-cost metals. At this concern, the latest scientific efforts have concentrated on the employment of non-prestigious 3d metals such as copper (Cu) [18,24], cobalt (Co) [19], nickel (Ni) [19] and iron (Fe) [19] as active centers in the nanocatalysts developed for the dehydrogenation of aqueous MeAB. Unfortunately, the majority of these low-cost nanocatalysts have provided either low activity [18,19,24] or reusability [19] performance. Hereof, the advance of low-cost nanocatalyst system that provides high reactivity and durability in MeAB hydrolysis is the wanted target for this important reaction.

With this motivation in mind, we have prepared cobalt nanoparticles supported on alumina (Al_2O_3) nanofibers (Co/Al_2O_3) by following two-steps procedure including double-solvent [31]followed by chemical reduction [32] methods and tested as a catalyst in MeAB hydrolysis. The characterization of the resulting material was carried out by using various spectroscopic and microscopic techniques, which shows that the formation of alumina nanofibers surface decorated cobalt(0) nanoparticles (3.9 ± 1.2 nm) by without damaging the crystallinity of the support material. The catalytic performance tests concerning reactivity and stability performed on the resulting Co/Al_2O_3 in the hydrolysis of MeAB reveal that Co/Al_2O_3 nanocatalyst effectively catalyzes hydrolytic dehydrogenation of MeAB by providing 3 equiv. of H_2 generation at an *initial* turnover frequency (TOF) value of 297 mol H_2/mol metal × h and room temperature. Recyclability experiments judged the stability of Co/Al_2O_3 nanocatalyst and concluded that cobalt nanoparticles decorated on alumina nanofibers are very stable against to agglomeration and leaching during the reaction.

Experimental section

Materials

Cobalt(II) chloride hexahydrate ($CoCl_2.6H_2O$), tetrahydrofuran (C_4H_8O), methylamine hydrochloride ($CH_3NH_2{\cdot}HCl$), alumina nanofibers (Al_2O_3 L < 20 nm × 100 μm), and diethyl ether ($(CH_3CH_2)_2O$) were acquired from Sigma. The synthesis of MeAB was done by following the literature procedure [17,18]. After synthesis and isolation, Co/Al_2O_3 samples were kept in atmosphere-controlled glove-box (Labsconco; H_2O < 3 ppm, O_2 < 2 ppm) to minimize their surface oxidation. Deionized water was provided from Milli-Q-WPS. Glassware types of equipment were washed with ethanol/acetone mixture and plentifully wetted afore drying in a vacuum oven.

Preparation protocol of cobalt nanoparticles supported on alumina nanofiber (Co/Al_2O_3)

Co/Al_2O_3 nanocatalyst was fabricated by following two-steps procedure including a double solvent method to impregnate

metal precursor onto the solid surface then, liquid-phase borohydride reduction of precatalyst. In a typical preparation route, 200 mg support material was transferred into a 10.0 mL n-hexane (dry), and sonicated approximately 20 min, then stirred at 1000 rpm for 1 h at 25 °C. Next, 1.0 mL aqueous $CoCl_2.6H_2O$ (23.92 mg, 0.1 mmol Co) was drop-wisely added over 15 min during the stirring for 2 h. Afterwards centrifugation (5000 rpm, 10 min), plentiful water washing (3 × 10 mL), the powdered form of sample was dried at 90 °C for 4 h. Next, a 5.0 mL $NaBH_4$ aqueous solution was poured into the powder sample, and the final solution was mixed for 30 min. Following, the mixture was taken into centrifugation for 5 min at 5000 rpm, washed with water/ethanol mixture and dried in a vacuum oven at 90 °C for 4 h. Finally, Co/Al_2O_3 nanocatalyst in the form of dark-gray powder was kept in the glove-box.

Characterization of Co/Al_2O_3 nanocatalyst

Cobalt (Co) loading of the samples in the form of % wt Co was found by inductively coupled plasma optical emission spectroscopy (ICP-OES; Perkin Elmer DRC II model) afterwards samples were entirely dissolved in a highly acidic solution. The crystallinity of Co/Al_2O_3 was surveyed via investigating their P-XRD patterns by using Rigaku Ultima-IV (Cu-Kα, 1.54 Å, 40 kV, 55 mA). The morphology of the resulting Co/Al_2O_3 was analyzed by using FE-SEM, TEM and HRTEM analyses. Firstly, FE-SEM images were obtained FE-SEM/Quanta 400 F. Then, we conducted TEM and HRTEM analyses, and TEM images were recorded on a JEOL (JEM-200 CX) TEM working at 120 kV, whereas HRTEM analyses were carried out on JEOL/JEM-2010F operational at 200 kV. Oxford EDX system equipped with Inca software to collect TEM-EDX spectrum. TEM/HRTEM samples were set by adding a drop of the catalyst solution on a TEM grid (Cu/C) followed by drying to remove solvent. XPS and HR-XPS spectra were taken on a PE-5800 XPS spectrometer (Al-Kα, 1486.6 eV, 15 kV, 350 W, 23.5 eV). NMR analyses were done on a Bruker Avance DPX (400.1 MHz for ^{1}H NMR; 128.2 MHz for ^{11}B NMR.

Co/Al_2O_3 catalyzed hydrolysis of methylamine-borane

The catalytic reactivity of Co/Al_2O_3 nanocatalyst was judged by determining the hydrogen generation rate (volume of H_2 to time), which was then transformed into the initial turnover frequency (mol H_2/mol Co × h). The volume of H_2 released from the catalytic reaction was measured via a gas burette method as described elsewhere [17–26]. In a typical test of the catalytic activity, Co/Al_2O_3 nanocatalyst was weighed and taken into the Schlenk, and then water was added followed by vigorous stirring ~15 min for the achievement of the thermal equilibrium. Ensuing, aqueous solution of MeAB was added fastly to start reaction at stirring speed of 1000 rpm.

Recyclability experiments

The catalytic durability of Co/Al_2O_3 nanocatalyst was evaluated by the use of the results of catalytic recyclability experiments, which were started with fresh Co/Al_2O_3 nanocatalyst and an aqueous MeAB solution at room temperature. Instantaneously after >90% conversion was achieved in 1st cycle, an additional same amount of substrate (MeAB) solution was taken into the catalytic reaction, providing more hydrogen evolution.

Results and discussion

Cobalt nanoparticles supported on alumina nanofibers: preparation and characterization

Cobalt nanoparticles decorated on alumina nanofibers (Co/Al_2O_3) were fabricated by two-steps procedure; (i) the impregnation of cobalt *pre*catalyst ($CoCl_2.6H_2O$) onto the alumina nanofiber surface by double solvent method [31] using n-hexane as hydrophobic solvent, (ii) next the room temperature reduction of Al_2O_3 surface impregnated *pre*-catalyst by aqueous sodium borohydride solution [32]. After washing and drying steps for purification to remove surface-bound chlorine (Cl^-) and metaborate (BO_2^-) anions, the resulting Co/Al_2O_3 nanocatalyst was isolated as a solid powdered sample. The characterization of Co/Al_2O_3 was started by examining P-XRD patterns of the product containing different amounts of cobalt. Fig. 1 displays P-XRD patterns of Al_2O_3 nanofibers along with Co/Al_2O_3 samples containing different amounts of cobalt (0.42, 1.02, 2.72 and 4.84 wt % Co loading) as found by ICP-OES analyses. The evaluation of P-XRD patterns obviously displays that the crystallinity of Co/Al_2O_3 samples at different Co loadings are indistinguishable to that of Al_2O_3 nanofiber and no new phases appear, thus signifying that Al_2O_3 nanofiber crystallinity leftovers undamaged at the end of the formation of Co/Al_2O_3. The nonappearance of any diffraction ascribed to cobalt nanoparticles can be explained by low loading wt % of Co onto host material. In the meantime the minor decline in the Bragg peak intensities of Co/Al_2O_3 samples by increasing of guest Co amounts can be attributed to the variation in the electron density due to the presence of cobalt nanoparticles on alumina surface and their contact through surface oxygen atoms and/or vacancies [33].

The surface elemental composition and the oxidation state of cobalt in Co/Al_2O_3 nanocatalyst (with 1.02 % wt Co loading) were examined by using XPS analyses. XPS spectrum of Co/Al_2O_3 taken as survey scan is depicted in Fig. 2(a) as seen from this spectrum acquired signals discloses that the surface composition comprised of Al, O, and Co. The oxidation state of Co was intensely investigated by HR-XPS analysis of Co/Al_2O_3. Fig. 2(b) displays HR-XPS spectrum taken at Co 2p core-level and its deconvoluted chemical states for Co/Al_2O_3, which shows that the existence of metallic Co (798 ev for $2p_{1/2}$, 781.5 eV for $2p_{3/2}$) along with minor amount of cobalt(II) oxide (CoO) (804 ev for $2p_{1/2}$, 787 eV for $2p_{3/2}$) [34,35]. The observation of oxide signals in HR-XPS spectra of transition metal nanoparticles is not a new phenomenon and usually caused from the surface oxidation of highly oxophilic transition metal nanoparticles for the duration of the sampling process [36]. The morphology, size, and dispersion of cobalt nanoparticles in Co/Al_2O_3 were inspected in terms of FE-SEM, SEM-EDX, TEM, and HRTEM studies. Fig. 3 shows FE-SEM images of Co/Al_2O_3 taken at various magnification values, and the inspection of these images indicate that (i) the observation of only

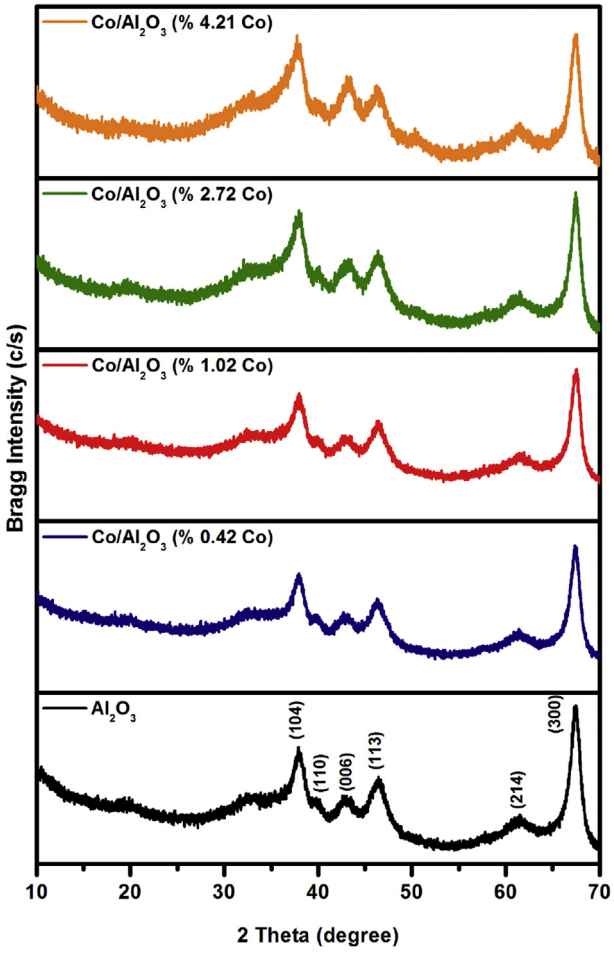


Fig. 1 – P-XRD patterns of Al_2O_3 and Co/Al_2O_3 samples at different cobalt loadings (0.42, 1.02, 2.72 and 4.84 wt % Co loading).

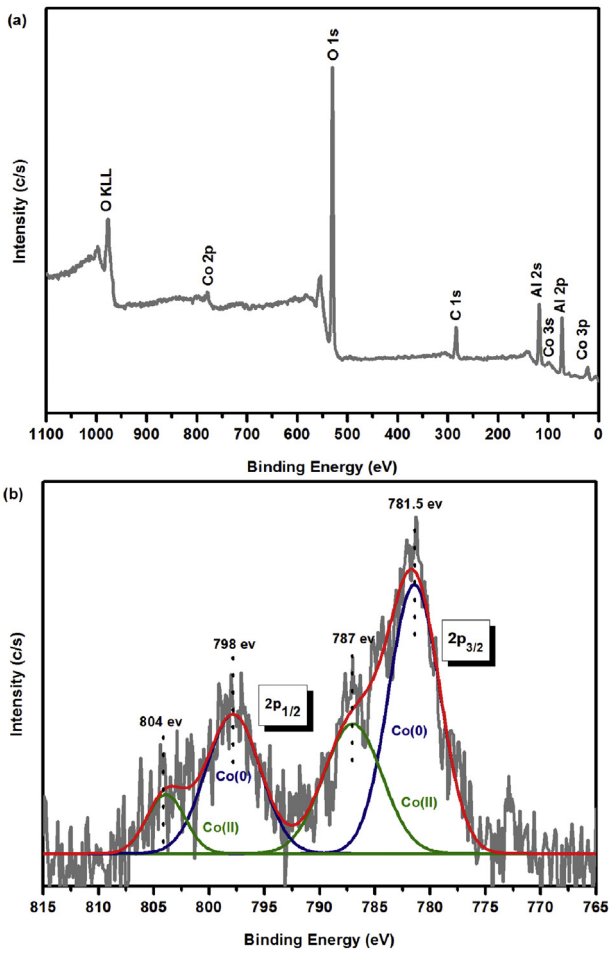


Fig. 2 – (a) Survey scan XPS spectrum and (b) Co 2p core level high-resolution XPS spectrum of Co/Al_2O_3.

Al_2O_3 nanofibers and preservation of fiber structure of Al_2O_3 upon formation of Co/Al_2O_3, (ii) no bulk cobalt shaped in observable size on the surface of Al_2O_3 nanofibers. Even though no bulk metallic cobalt is detected on the surface of Al_2O_3 nanofibers, SEM-EDX spectrum (Fig. S1 in the Supporting Information) as well as IC-OES analyses, point to the existence of cobalt in material, which suggests the formation of cobalt nanoparticles in small-sized (<50 nm) regime in Co/Al_2O_3 nanocatalyst.

Next, the same Co/Al_2O_3 sample (with 1.02 % wt Co loading) was further analyzed by TEM and HRTEM microscopic techniques. TEM images of Co/Al_2O_3 nanocatalyst are illustrated in Fig. 4 (a)-(b), the scrutiny of them undoubtedly shows that the existence of small sized Co nanoparticles along with some clumped Co nanoparticles (circled in Fig. 4(a)). The mean particle size of non-clumped cobalt nanoparticles was estimated to be 3.9 ± 1.2 nm through an NIH image program [37], whereby 80 particles were considered (Fig. 4(c)). The crystallinity of the resulting cobalt nanoparticles was investigated by HRTEM, Fig. 4(d) shows HRTEM image of Co/Al_2O_3 nanocatalyst that shows the formation of highly crystalline cobalt nanoparticles and the crystalline fringe distance of cobalt nanoparticle was measured to be 0.205 nm, which can be ascribed to (111) plane of *fcc* cobalt [38].

Catalytic hydrolysis of MeAB in the presence Co/Al_2O_3 nanocatalyst

The catalytic nature of metal-free Al_2O_3 nanofiber and the effect of cobalt loading and oxidized Co species on Co/Al_2O_3 activity

Before starting the catalytic performance tests, one should check the catalytic nature of the support material in the target catalytic reaction under identical conditions to express net reactivity of the guest metal nanoparticles in nanocatalysis. For that reason, firstly we checked the activity of metal-free Al_2O_3 nanofibers in the MeAB hydrolysis at room temperature, and the result of this experiment revealed that neat Al_2O_3 nanofibers are catalytically inactive in this catalytic transformation. Then, control tests were done to realize the effect of cobalt loading on Co/Al_2O_3 activity and optimize cobalt loading on Co/Al_2O_3 nanocatalyst. In these experiments, the catalytic activity of Co/Al_2O_3 nanocatalyst with various cobalt loadings (0.42, 1.02, 2.72 and 4.84 wt % Co) was examined in MeAB hydrolysis under alike conditions ([Co], [MeAB] and temperature). The results gained from these experiments are

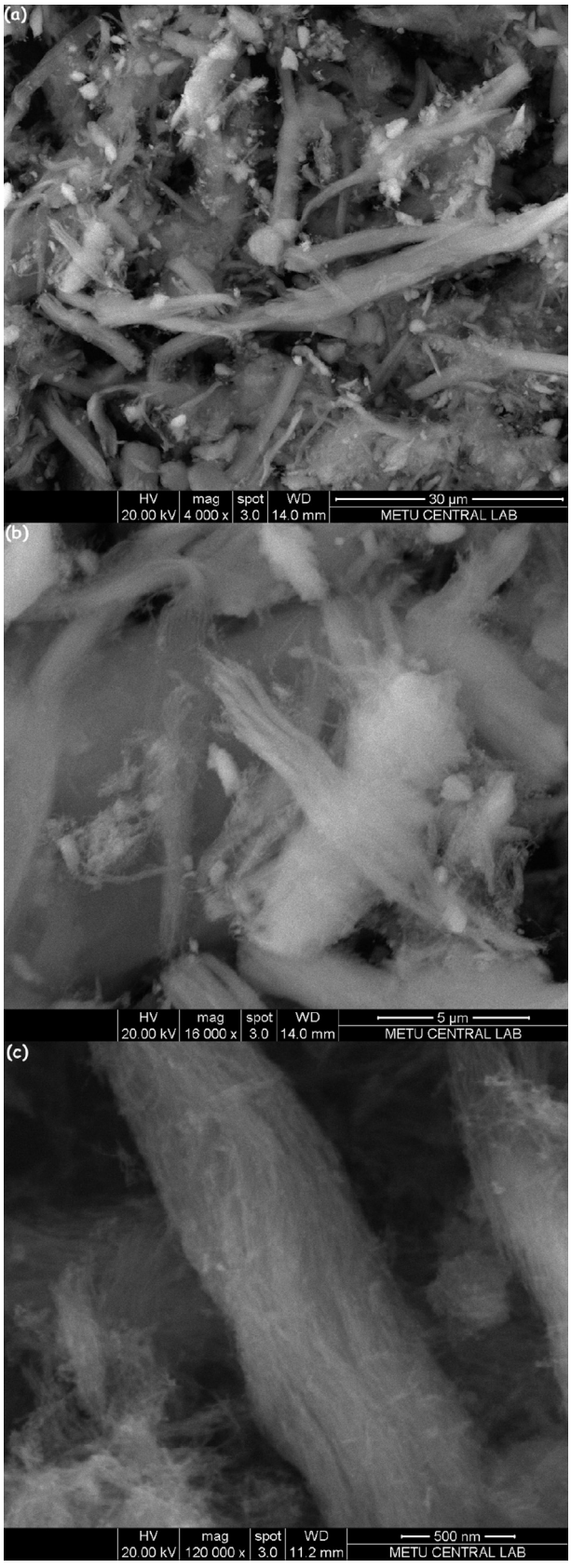


Fig. 3 – (a–c) FE-SEM images of Co/Al_2O_3 at different magnification ratios.

summarized in Fig. 5 and as easily understood the highest conversion and activity performance was achieved by Co/Al_2O_3 sample that comprised of 1.02 % wt Co loading. The *initial* turnover frequency (TOF) values were found to be 106, 297, 203 and 145 mol H_2/mol metal × h for Co/Al_2O_3 nanocatalysts containing 0.42, 1.02, 2.72 and 4.84 wt % Co, respectively. The distinction observed in the catalytic activity of Co/Al_2O_3 samples (Fig. 5) reflects the accessibility of cobalt nanoparticles in Co/Al_2O_3 by MeAB so that cobalt nanoparticles in Co/Al_2O_3 sample containing 1.02 % wt Co are most readily accessible. Additionally, the increase in the size of cobalt nanoparticles, especially at high Co loadings (2.72 and 4.84 wt % Co) can also explain the observation of low activities with respect to that of obtained by Co/Al_2O_3 sample containing 1.02 % wt Co. Indeed, the informative TEM image (Fig. 5) taken from Co/Al_2O_3 sample containing 4.84 % wt Co confirms that formation of larger size cobalt nanoparticles (4.9 ± 1.6 nm) in this sample that explains its lower activity than that of Co/Al_2O_3 sample containing 1.02 % wt Co. It is worth noting that, the other test reported hereafter Co/Al_2O_3 nanocatalyst with 1.02 % wt Co loading was used unless otherwise stated. As well as the quantification of volume of hydrogen, the completion of the catalytic transformation was also checked by ^{11}B NMR spectroscopy. The ^{11}B-{^1H}-NMR spectrum of the aliquot recovered at the end of the catalytic reactions shows that $MeNH_2BH_3$ ($\delta = -19$ ppm, q) is wholly transformed into $(MeNH_3)BO_2$ ($\delta = -13.2$ ppm, s) (Fig. S2 in the Supporting Information).

Another control experiment was performed for the clarification of active catalytic species (Co or Co(II), which was detected in XPS analyses), and in a separate control experiment the nature of active species was investigated by checking and comparing the catalytic activities of Co/Al_2O_3 and Co_xO_y/Al_2O_3, which was fabricated through the heating of Co/Al_2O_3 under O_2 stream, in the hydrolysis of MeAB under identical conditions (Fig. S3 in the Supporting Information). Expectedly, after an induction time period (required for the reduction of oxidized cobalt species to metallic cobalt) Co_xO_y/Al_2O_3 catalyzes hydrolysis of MeAB at almost same reactivity with Co/Al_2O_3 so the result of this experiment indicates that the catalytically active species were comprised of metallic cobalt (Co(0)).

Effect of supporting catalytically active cobalt; comparison of the catalytic activities of $CoCl_2.6H_2O$ precatalyst and Co/Al_2O_3

In order to understand stabilizing effect of Al_2O_3 nanofiber support on catalytically active Co species, which were formed at the nucleation step during the reduction of $CoCl_2.6H_2O$ precatalyst, we performed two groups of experiments in which the catalytic reactivities of $CoCl_2.6H_2O$ precatalyst and Co/Al_2O_3 sample containing 1.02 % wt Co were monitored up to two catalytic recycles in the hydrolysis of MeAB. The results of these experiments are demonstrated in Fig. 6. Throughout the reduction of Co(II) to Co(0) the sole stabilizing agent in the aqueous solution is the weakly coordinating chloride anion and it has recently been reported that chloride anion as electrostatic stabilizing agent cannot afford enough stabilization to colloidal metal nanoparticles [[39]]. Hence cobalt species formed via the reduction from $CoCl_2.6H_2O$ precatalyst could not preserve their remarkable activity observed in the first catalytic cycle due to the formation of bulky Co that

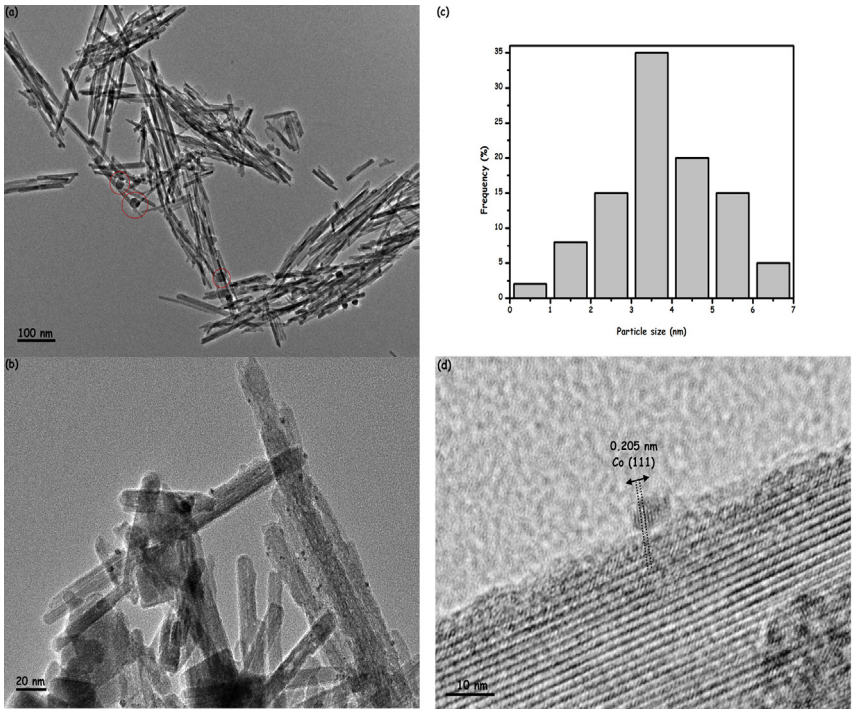


Fig. 4 – (a,b) TEM images and (c) the size histogram of Co/Al_2O_3 (d) HRTEM image of Co/Al_2O_3.

precipitated out from the solution (Fig. S4 in the Supporting Information) [40,41]. For that reason, almost no hydrogen evolution was observed for the second catalytic cycle in the MeAB hydrolysis, whereas Co/Al_2O_3 nanocatalyst retains >80% initial activity at the second catalytic cycle. These results are indicative of the stabilizing effect of Al_2O_3 nanofiber plus the importance of the size of catalytically active metal in catalysis.

Effect of methylamine-borane [MeAB] and cobalt [Co] concentrations on the rate of Co/Al_2O_3 catalyzed hydrolytic dehydrogenation of MeAB

To clarify rate expression for Co/Al_2O_3 catalyzed hydrolytic dehydrogenation of MeAB we conducted two groups of experiments in which the effect of cobalt and MeAB concentrations on the rate of catalytic transformation was investigated. Fig. 7 shows mole of H_2/mole MeAB versus time plot for Co/Al_2O_3 catalyzed MeAB hydrolysis (0.82 mmol and kept constant in all experiments) at room temperature starting with different cobalt concentrations ([Co] = 0.43, 0.86, 1.29 and 1.72 mM); as predictable hydrogen generation rate increases owing to increase of cobalt concentration. The rate of hydrogen generation versus cobalt concentration (in log. scale; inset in Fig. 7) plot has a line with a slope of 1.12, revealing that Co/Al_2O_3 catalyzed hydrolysis of MeAB occurs in the first order relative to the cobalt concentration.

Next, in the second bunch of experiments, we kept cobalt concentration constant and varied initial substrate ([MeAB]) concentration, and their outcomes are given in Fig. 8, which reveals that the rate of hydrogen generation is not differing too much in the substrate concentration range of 41–82 mM but remarkably increases at [MeAB] > 82 mM. Under these circumstances, the slope of the line (Fig. 8 inset) fitted from the log. scale plot of hydrogen generation rate versus MeAB concentration was found to be 0.5 revealing that Co/Al_2O_3 catalyzed hydrolysis of MeAB takes place in half order in respect of MeAB concentration, which is different from zero-order dependence to AB in AB methanolysis on CoPd alloy nanoparticles [42], first-order dependence to AB in AB methanolysis on Ru nanoparticles [43] but is similar to AB in AB hydrolysis over Ni nanoparticles [44] and MeAB in MeAB methanolysis on Rh nanoparticles [25].

Effect of temperature on the rate of Co/Al_2O_3 catalyzed hydrolytic dehydrogenation of MeAB

Fig. 9 shows mole of H_2/mole MeAB versus time graph for Co/Al_2O_3 catalyzed MeAB hydrolysis at the different temperatures as one can expect the enhancement in rate of hydrogen generation is observed depending on the increase of temperature. The *initial* hydrogen generation rates for Co/Al_2O_3 catalyzed MeAB hydrolysis at 15, 25, 35 and 45 °C were found to be 0.57, 1.56, 1.88 and 3.63 mL $H_2 \times min^{-1}$, respectively. These values were used to get Arrhenius plot (inset Fig. 9) that tells us the activation energy of Co/Al_2O_3 catalyzed MeAB hydrolysis is 44.23 kJ/mol, and this observed activation energy value is lower than those of provided by $Cu_{0.2}@Co_{0.8}$/r-GO (55.9 kJ/mol) [18], Ru@Ni/r-GO (57 kJ/mol) [20] and Ru/MCM-41 (47.6 kJ/mol) [22].

The activity values on the order of *initial* TOF values were also found from Fig. 9, and *initial* TOF values were estimated to be 112, 297, 346 and 647 mol H_2/mol metal × h at 15, 25, 35, and 45 °C, respectively. The initial TOF value gained by Co/Al_2O_3 nanocatalyst (297 mol H_2/mol metal × h) is higher than previously reported catalytic systems such as $Cu_{0.2}@Co_{0.8}$/r-GO (138 mol H_2/mol metal × h) [18], Cu/nano-MIL-101 (247 mol H_2/mol metal × h) [24], and $Ag_{0.1}@Co_{0.45}Ni_{0.45}$/r-GO (210 mol H_2/mol metal × h) [17] for the same catalytic transformation. This remarkable catalytic activity obtained by Co/Al_2O_3 nanocatalyst in MeAB hydrolysis can be attributed to small size and

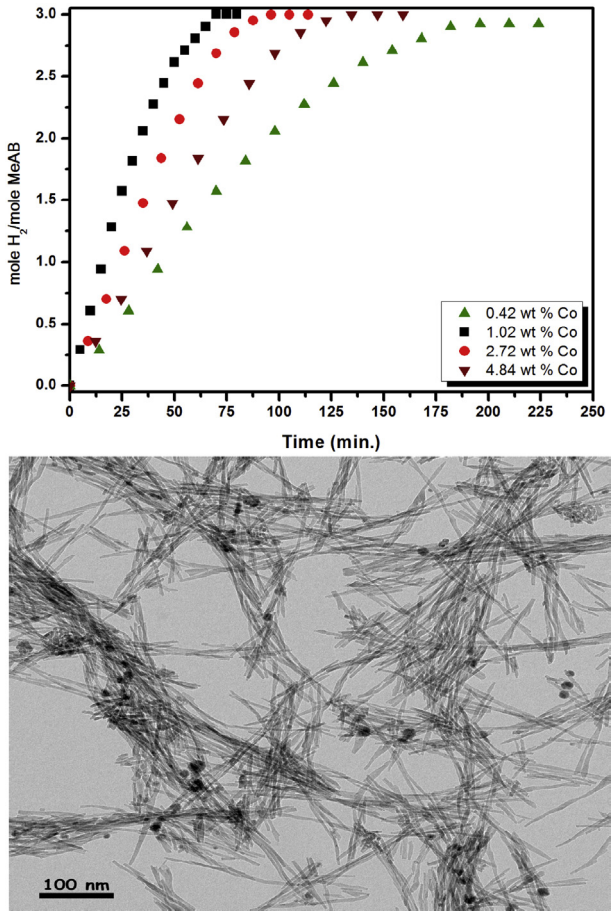


Fig. 5 – Mole of H_2/mole MeAB versus time (min.) graph for Co/Al_2O_3 nanocatalyst with various cobalt loadings (0.42, 1.02, 2.72 and 4.84 wt % Co) catalyzed (in all 12.9 μmol Co) hydrolytic dehydrogenation of MeAB (0.82 mmol) at 25 °C and TEM image of Co/Al_2O_3 nanocatalyst contains 4.84 wt % Co.

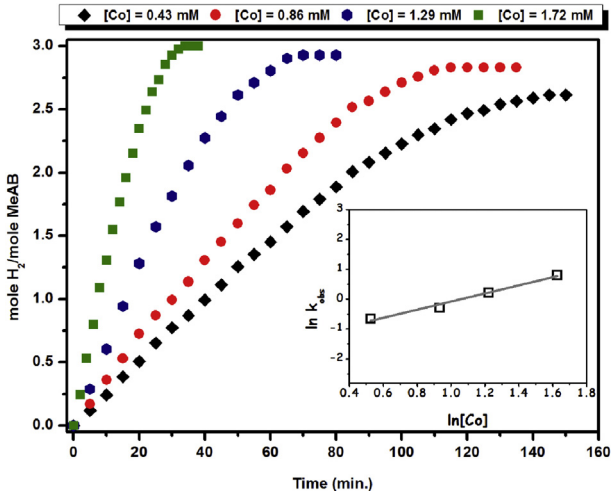


Fig. 7 – Mole of H_2/mole MeAB versus time (min.) graphs for the hydrolysis of MeAB (in all [MeAB] = 0.82 mM) at 25 °C catalyzed by Co/Al_2O_3 nanocatalyst containing different amounts of cobalt ([Co] = 0.43, 0.86, 1.29 and 1.72 mM).

high dispersion of cobalt nanoparticles on host Al_2O_3 nanofiber surface plus strong metal support interaction between guest cobalt nanoparticles and host Al_2O_3 nanofiber support material [45,46].

Catalytic durability of Co/Al_2O_3 nanocatalyst in the hydrolysis of MeAB

The catalytic durability of Co/Al_2O_3 nanocatalyst in the catalytic hydrolysis of MeAB was inspected by testing its recyclability performance. As illustrated in Fig. 10, Co/Al_2O_3 nanocatalyst retains 97% of its original catalytic performance in conversion (97% conversion at 5th recycle) by providing 72% of its natural activity at 5th recycle in MeAB hydrolysis. The initial TOF values for 1st, 2nd, 3rd, 4th and 5th recycles were found to be 297, 252, 238, 227 and 213 mol H_2/mol metal × h,

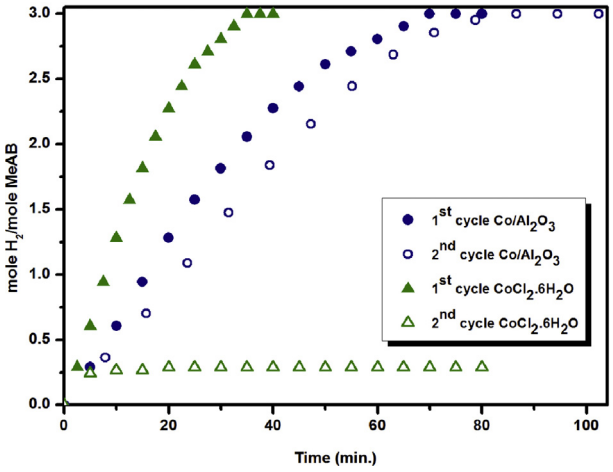


Fig. 6 – Mole of H_2/mole MeAB versus time (min.) graphs for recyclability of $CoCl_2.6H_2O$ precatalyst and Co/Al_2O_3 nanocatalyst (in all 12.9 μmol Co) in the catalytic hydrolysis of MeAB (0.82 mmol) at 25 °C.

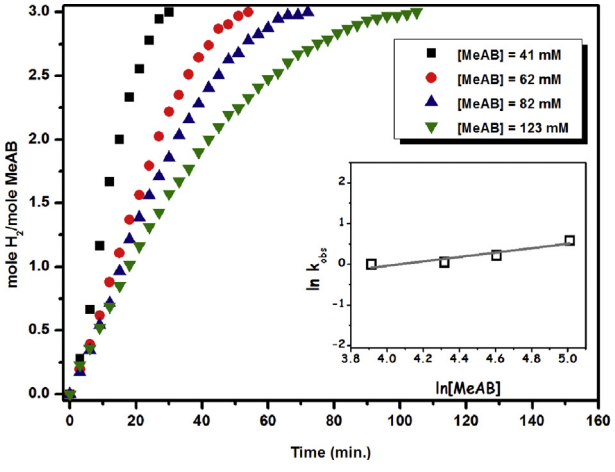


Fig. 8 – Mole of H_2/mole MeAB versus time (min.) graphs for Co/Al_2O_3 catalyzed (in all [Co] = 1.29 mM) MeAB hydrolysis at different MeAB concentrations ([MeAB] = 0.41, 062, 0.82 and 123 mM) and room temperature.

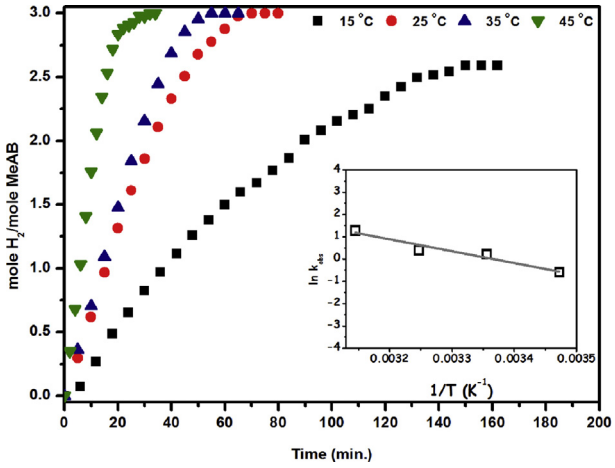


Fig. 9 – Mole of H_2/mole MeAB versus time (min.) graphs for Co/Al_2O_3 catalyzed ([Co] = 1.29 mM) in the hydrolysis of MeAB ([MeAB] = 0.82 mM) at different temperatures and Arrhenius graph (inset).

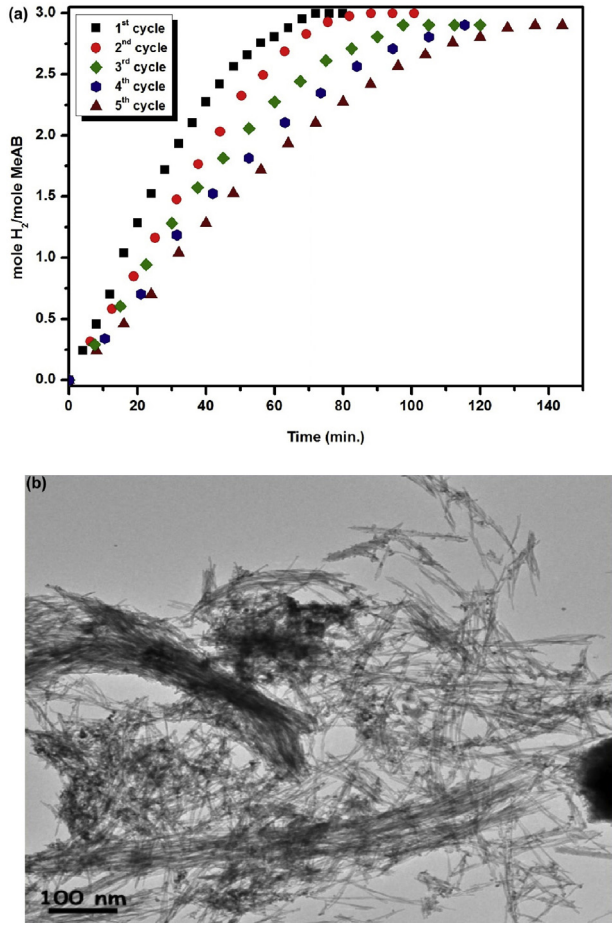


Fig. 10 – (a) Mole of H_2/mole MeAB versus time (min.) graphs for recyclability of Co/Al_2O_3 nanocatalyst ([Co] = 1.29 mM) in the hydrolysis of MeAB ([MeAB] = 0.82 mM) up to five catalytic recycles and (b) TEM image of Co/Al_2O_3 nanocatalyst recovered from 5th catalytic recycle.

respectively. The observed decline in the catalytic performance of Co/Al_2O_3 nanocatalyst in both conversion and activity was inspected by carrying out analyses on the reused Co/Al_2O_3 nanocatalyst. The TEM image of Co/Al_2O_3 nanocatalyst recovered from the 5th catalytic recycle (inset Fig. 10) indicative of clumping of both Al_2O_3 nanofiber and surface-bound cobalt nanoparticles that elucidates the reason of observed decrease in the catalytic performance. In addition, the slight decrease in catalytic activity in subsequent runs may also be attributed to the passivation of cobalt nanoparticles surface by increasing the concentration of boron products, *e.g.* metaborate, which decreases accessibility of active sites [47,48].

It should be underlined that the leaching possibility of guest cobalt nanoparticles from Al_2O_3 nanofiber surface to aqueous solution during these experiments was also examined by carrying out ICP-OES investigates on reaction sample solutions taken at the finishing of 1st, 3rd and 5th recycle, in none of them, cobalt was detected. This result is confirming that the retention of cobalt nanoparticles on Al_2O_3 nanofiber support material and there is no leaching of cobalt into the aqueous reaction solution. Additionally, the crystallinity of the host material Al_2O_3 nanofibers was also checked at the end of the recyclability experiment by considering P-XRD pattern of Co/Al_2O_3 nanocatalyst recovered from 5th catalytic recycle (Fig. S5 in the Supporting Information). It shows that the crystallinity of Al_2O_3 nanofibers retained intact at the end of these experiments. Bearing in mind of results of these experiments, one can conclude that Co/Al_2O_3 nanocatalyst is acting as not only active but also durable nanocatalyst for the catalytic hydrolysis of MeAB.

Conclusions

This presented study is focused on the development cobalt nanoparticles decorated on alumina nanofibers and their employment as heterogeneous catalyst in the hydrolysis of MeAB and has given following understandings; (*i*) Co/Al_2O_3 nanocatalyst can fabricated through the double solvent method followed by borohydride reduction technique carried out at room temperature, (*ii*) The formation of highly dispersed cobalt nanoparticles (3.9 ± 1.2 nm) on Al_2O_3 nanofibers surface have been confirmed by using characterization techniques, (*iii*) Co/Al_2O_3 was found to be an active catalyst in the hydrolytic dehydrogenation of MeAB, which provides TOF value of 297 mol H_2/mol metal × h at room temperature and 3 equiv. H_2 generation, (*iv*) Moreover, Co/Al_2O_3 nanocatalyst offers acceptable catalytic durability during the course of the recyclability experiments.

In summary, Co/Al_2O_3 nanocatalyst is readily available by a low-cost and straightforward procedure and found to be an active and stable catalyst in the hydrolysis of MeAB.

Acknowledgment

The authors acknowledge Research Fund of Van Yuzuncu Yıl University Scientific Research Office (Project ID: FDP-2017-6559) for their funding.

Appendix A. Supplementary data

Supplementary data to this article can be found online at https://doi.org/10.1016/j.ijhydene.2019.02.088.

REFERENCES

[1] Turner JA. Sustainable hydrogen production. Science 2004;305:972–4.
[2] Hetland J, Mulder G. In search of a sustainable hydrogen economy: how a large-scale transition to hydrogen may affect the primary energy demand and greenhouse gas emissions. Int J Hydrogen Energy 2007;32:736–47.
[3] Laurent C, Morishima R, Suzuki H, Lelay M. Hydrogen storage in high surface area carbon nanotubes produced by catalytic chemical vapor deposition. J Phys Chem B 2004;108:12718–23.
[4] Dong J, Wang X, Xu H, Zhao Q, Li Q. Hydrogen storage in several microporous zeolites. Int J Hydrogen Energy 2007;32:4998–5004.
[5] Tranchemontagne DJ, Park KS, Furukawa H, Eckert J, Knobler CB, Yaghi OM. Hydrogen storage in new metal–organic frameworks. J Phys Chem C 2012;116:13143–51.
[6] McKeown NB, Budd PM. Polymers of intrinsic microporosity (PIMs): organic materials for membrane separations, heterogeneous catalysis and hydrogen storage. Chem Soc Rev 2006;35:675–83.
[7] Singh SK, Zhang XB, Xu Q. Room-temperature hydrogen generation from hydrous hydrazine for chemical hydrogen storage. J Am Chem Soc 2009;131:9894–5.
[8] Sakintuna B, Darkrim FL, Hirscher M. Metal hydride materials for solid hydrogen storage: a review. Int J Hydrogen Energy 2007;32:1121–40.
[9] Hamilton CW, Baker T, Staubitz A, Manners I. B-N compounds for chemical hydrogen storage. Chem Soc Rev 2009;38:279–93.
[10] Akbayrak S, Ozkar S. Ammonia-borane as hydrogen storage materials. Int J Hydrogen Energy 2018;43:18592–606.
[11] Demirci UB. Ammonia borane, a material with exceptional properties for chemical hydrogen storage. Int J Hydrogen Energy 2017;42:9978–10013.
[12] Umegaki T, Yan JM, Zhang XB, Shioyama H, Kuriyama N, Xu Q. Boron- and nitrogen-based chemical hydrogen storage materials. Int J Hydrogen Energy 2009;34:2303–11.
[13] Turner J, Sverdrup G, Mann K, Maness PG, Kroposki B, Ghirardi M, Evans RJ, Blake D. Renewable hydrogen production. Int J Energy Res 2008;32:379–407.
[14] Karkamkar A, Aardahl C, Autrey T. Recent developments on hydrogen release from ammonia borane. Mater. Matters 2007;2:6–9.
[15] Jiang HL, Xu Q. Catalytic hydrolysis of ammonia borane for chemical hydrogen storage Catal. Tod 2011;170:56–63.
[16] Staubitz A, Sloan ME, Robertson APM, Friedrich A, Schneider S, Gates PJ, Schmedt J, Manners I. Catalytic dehydrocoupling/dehydrogenation of N-Methylamine-Borane and ammonia-borane: synthesis and characterization of high molecular weight polyaminoboranes. J Am Chem Soc 2010;132:13332–45.
[17] Yang L, Su J, Meng XY, Luo W, Cheng GZ. In-situ synthesis of graphene supported Ag@CoNi core-shell nanoparticles as highly efficient catalysts for hydrogen generation from hydrolysis of ammonia borane and methylamine borane. J Mater Chem A 2013;1:10016–23.
[18] Du YS, Cao N, Yang L, Luo W, Cheng GZ. One-step synthesis of magnetically recyclable rGO supported Cu@Co core-shell nanoparticles: highly efficient catalysts for hydrolytic dehydrogenation of ammonia borane and methylamine borane. New J Chem 2013;37:3035–42.
[19] Yang L, Luo W, Cheng GZ. Graphene-supported Ag-based core-shell nanoparticles for hydrogen generation in hydrolysis of ammonia borane and methylamine borane. ACS Appl Mater Interfaces 2013;5:8231–40.
[20] Cao N, Su J, Luo W, Cheng GZ. Hydrolytic dehydrogenation of ammonia borane and methylamine borane catalyzed by graphene supported Ru@Ni core-shell nanoparticles. Int J Hydrogen Energy 2014;39:426–35.
[21] Cao N, Su J, Luo W, Cheng GZ. Graphene supported Ru@Co core-shell nanoparticles as efficient catalysts for hydrogen generation from hydrolysis of ammonia borane and methylamine borane. Catal Commun 2014;43:47–51.
[22] Wen L, Zheng Z, Luo W, Cai P, Cheng GZ. Ruthenium deposited on MCM-41 as efficient catalyst for hydrolytic dehydrogenation of ammonia borane and methylamine borane. Chin Chem Lett 2015;26:1345–50.
[23] Khalily MA, Yurderi M, Haider A, Bulut A, Patil B, Zahmakiran M, Uyar T. Atomic layer deposition of ruthenium nanoparticles on electrospun carbon nanofibers: a highly efficient nanocatalyst for the hydrolytic dehydrogenation of methylamine borane. ACS Appl Mater Interfaces 2018;10:26162–9.
[24] Baguc IB, Ertas IE, Yurderi M, Bulut A, Zahmakiran M, Kaya M. Nanocrystalline metal organic framework (MIL-101) stabilized copper nanoparticles: highly efficient nanocatalyst for the hydrolytic dehydrogenation of methylamine borane. Inorg Chim Acta 2018;483:431–9.
[25] Kanat M, Karatas Y, Gulcan M, Anıl B. Preparation and detailed characterization of zirconia nanopowder supported rhodium (0) nanoparticles for hydrogen production from the methanolysis of methylamine-borane in room conditions. Int J Hydrogen Energy 2018;43:22548–56.
[26] Gulcan M, Karatas Y. Synthesized polyvidone-stabilized Rh(0) nanoparticles catalyzed the hydrolytic dehydrogenation of methylamine-borane in ambient Conditions. New J Chem 2017;41:11839–45.
[27] Bowden ME, Brown IWM, Gainsford GJ, Wong H. Structure and thermal decomposition of methylamine borane. Inorg Chim Acta 2008;361:2147–53.
[28] Zahmakiran M, Ozkar S. Metal nanoparticles in liquid phase catalysis; from recent advances to future goals. Nanoscale 2011;3:3462–81.
[29] Cushing BL, Kolesnichenko L, Connor CJ. Recent advances in the liquid-phase syntheses of inorganic nanoparticles. Chem Rev 2004;104:3893–996.
[30] Ozkar S, Finke RG. Nanocluster formation and stabilization fundamental studies: ranking commonly employed anionic stabilizers via the development, then application, of five comparative criteria. J Am Chem Soc 2002;124:5796–895.
[31] Zhu QL, Li J, Xu Q. Immobilizing metal nanoparticles to metal-organic frameworks with size and location control for optimizing catalytic performance. J Am Chem Soc 2013;135:10210–3.
[32] White RJ, Luque R, Budain VL, Clark JH, Macquarrie DJ. Supported metal nanoparticles on porous materials. Methods and applications. Chem Soc Rev 2009;38:481–97.
[33] Taglauer E, Knözinger H. Characterization of supported catalyst systems with surface spectroscopies. Phys Status Solidi 1995;192:465–75.
[34] Xia H, Xia WC, Zhang LJ, Yang H, Yang SP. Preparation and magnetic properties of cobalt nanoparticles with dendrimers as templates. Mater Chem Phys 2010;121:342–8.

[35] Bulut A, Yurderi M, Ertas IE, Celebi M, Kaya M, Zahmakiran M. Carbon dispersed copper-cobalt alloy nanoparticles: a cost-effective heterogeneous catalyst with exceptional performance in the hydrolytic dehydrogenation of ammonia-borane. Appl Catal B Environ 2016;180:121–9.
[36] Lee JM, Kim JW, Lim JS, Kim TJ, Kim SD, Park SY, Lee YS. X-ray photoelectron spectroscopy study of cobalt supported multi-walled carbon nanotubes prepared by different precursors. Carbon Sci 2007;8:120–6.
[37] Hutchison JE, Woehrle GH, Ozkar S, Finke RG. Analysis of nanoparticle transmission electron microscopy data using a public- domain image-processing program, image. Turkish J.Chem. 2006;30:1–13.
[38] Haipeng L, Yue L, Yongguang Z, Chunyong L, Hongshui W, Baoe L, Desmond A, Zhumabay B. Fabrication and properties of carbon- encapsulated cobalt nanoparticles over NaCl by CVD. Nanoscale Res Lett 2016;11:1–9.
[39] Ozkar S, Finke RG. Nanocluster formation and stabilization fundamental studies: ranking commonly employed anionic stabilizers via the development, then application, of five comparative criteria. J Am Chem Soc 2002;124:5796–810.
[40] Arzac GM, Hufschmidt D, Jiménez De Haro MC, Fernandez A, Sarmiento B, Jimenez AB, Jimenez MM. Deactivation, reactivation and memory effect on Co–B catalyst for sodium borohydride hydrolysis operating in high conversion conditions. Int J Hydrogen Energy 2012;37:14373–81.
[41] Arzac GM, Rojas TC, Fernandez A. Boron compounds as stabilizers of a complex microstructure in a Co-B based catalyst for $NaBH_4$ hydrolysis. ChemCatChem 2011;3:1305–13.
[42] Sun DH, Mazumder V, Metin O, Sun SH. Methanolysis of ammonia-borane by CoPd nanoparticles. ACS Catal 2012;2:1290–5.
[43] Dai HB, Kang XD, Wang P. Ruthenium nanoparticles immobilized in montmorillonite used as catalyst for methanolysis of ammonia borane. Int J Hydrogen Energy 2010;35:10317–23.
[44] Zhou LM, Zhang TR, Tao ZL, Chen J. Ni nanoparticles supported on carbon as efficient catalysts for the hydrolysis of ammonia borane. Nano Res 2014;7:774–81.
[45] Ivanova AS, Slavinskaya EM, Gulyaev RV, Zaikovskii VI, Stonkus OA, Danilova IG, Plyasova M, Polukhina A, Boronin AI. Metal–support interactions in Pt/Al2O3 and Pd/Al2O3 catalysts for CO oxidation. Appl Catal B Environ 2010;97:57–71.
[46] Ilieva L, Petrova P, Pantaleo G, Zanella R, Sobczak JW, Lisowski W, Kaszkur Z, Munteanu G, Yordanova I, Liotta LF, Venezia AM, Tabakova T. Alumina supported Au/Y-doped ceria catalysts for pure hydrogen production via PROX. Int J Hydrogen Energy 2019;44:233–45.
[47] Jaska CA, Clark TJ, Clendenning SB, Grozea D, Turak A, Lu Z-H, Manners I. Poisoning of heterogeneous, late transition metal dehydrocoupling catalysts by boranes and other group 13 hydrides. J Am Chem Soc 2005;127:5116–24.
[48] Mousa G, Moury R, Demirci UB, Miele P. Borates in hydrolysis of ammonia borane. Int J Hydrogen Energy 2013;38:7888–95.